










Microwave energy-based manufacturing of hollow carbon nanospheres decorated with carbon nanotubes or metal oxide nanowires

Selcuk Poyraz^{1,2,*} , Jonathan Cook¹ , Zhen Liu³, Lin Zhang⁴ , Amit Nautiyal¹ , Britta Hohmann¹ , Solveig Klamt¹ , and Xinyu Zhang¹ 

¹Department of Chemical Engineering, Auburn University, Auburn, AL 36849, USA

²Department of Textile Engineering, Faculty of Engineering, Adiyaman University, 02040 Altinsehir, Adiyaman, Turkey

³Department of Physics and Engineering, Frostburg State University, Frostburg, MD 21532-2303, USA

⁴Electronic Materials Research Laboratory, Key Laboratory of the Ministry of Education and International Center for Dielectric Research, School of Electronic and Information Engineering, Xi'an Jiaotong University, Xi'an 710049, China

Received: 5 December 2017

Accepted: 26 May 2018

Published online:

5 June 2018

© Springer Science+Business Media, LLC, part of Springer Nature 2018

ABSTRACT

Nanostructured hollow carbon spheres (HCNSs), with either carbon nanotube (CNT) or metal oxide nanowire (MONW) decoration on their surface, were synthesized as building materials with a great potential for the next-generation advanced applications. A well-established, polymeric latex NS synthesis method and a simply modified version of a microwave (MW) energy-based carbonization approach, i.e., Poptube, were systematically combined to obtain these HCNSs. Through this simple, facile, affordable and easily scalable “combined synthesis method,” it was managed to successfully produce HCNSs with unique morphological, spectroscopic, thermal and elemental features, all of which were strongly supported by both various material characterization test results and the relevant previous literature data. Thus, it is believed that the as-synthesized CNT or MONW decorated HCNSs (CNT-MONW/HCNS) from the above-mentioned method would soon become the materials of preference for the next-generation advanced applications in various science and engineering fields.

Introduction

Recently, bare HCSs or their core-shell derivatives combining hollow and porous carbon nanostructures have received increasing attention in various fields of science and engineering such as catalysis, composites

for high energy storage (super-capacitance, lithium-ion/sulfur battery (LIB), fuel cell etc.), water treatment, magnetic resonance imaging (MRI) and electromagnetic interference (EMI) shielding due to their advantageous features such as high electrochemical reactivity, low density and long-term thermo/

Address correspondence to E-mail: spoyraz@adiyaman.edu.tr

mechanical stability [1–8]. In terms of different structure and type of materials, the core–shell concept is generally presented as core-A@shell-B in different ways, such as metal@polymer, metal@carbon, carbon@carbon and metal-oxide@carbon [6–9]. In such systems, the hollow spheres (or shell) usually act as a barrier to prevent the encapsulated or decorated nanostructures from coalescence and also provide them a vast interstitial space for their accommodation in large quantities, which is crucial to improve and optimize the overall performance of such materials in different applications.

To date, several methods have been proposed to prepare various HCS composites decorated with different nanomaterials and morphologies [10–12], including the template-assisted methods [13, 14], precursor-controlled carbonization [15], solvo/thermal methods [16], self-assembly by using soft templates [17], pyrolysis [18], and chemical vapor deposition with a relevant catalyst [19]. For this purpose, polymeric materials, i.e., conducting polymers (CPs), have been commonly used as carbon precursors [20–23]. The as-obtained HCSs from those approaches were often benefited as the electrode materials for energy storage applications via combining the advantages of nanostructured carbon materials' design and the unique electrochemical features of the decorating nanomaterials in one structure. However, since the as-prepared HCSs' average diameter usually falls in the micron range [24, 25], it causes a restriction on their total specific active surface area [11, 26–28]. Thus, in order to address the functional material needs for the above mentioned applications' vast potential and to tackle the so-called size distribution problem; a simple, facile, easily scalable and low-cost method needs to be urgently developed to obtain HCNSs with larger surface area and smaller diameters.

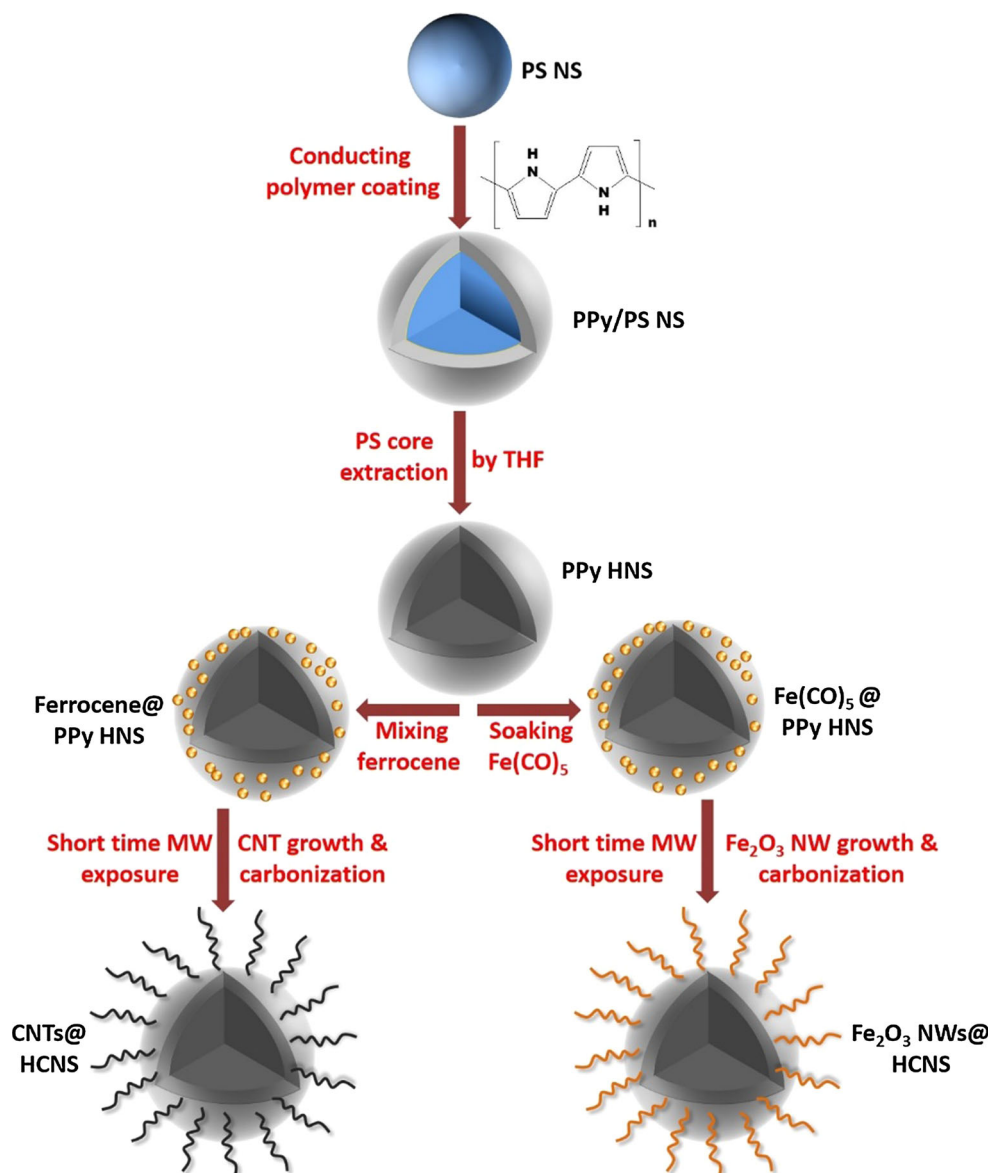
In this manner, along with the combination of different precursor chemicals, polypyrrole (PPy) had been commonly used as an active material to achieve superior performances in nanocomposites [29]. Among CPs, PPy has been one of the most extensively studied members due to its many advantages such as its simple and straightforward preparation at ambient conditions, low-cost and high polymerization yield, unique electrochemical properties, relatively high conductivity, and long-term thermal and environmental stability with good processability [30, 31]. Thus, throughout the last decade, various

nanostructured PPy morphologies from zero dimensional (0D) nanogranules to three-dimensional (3D) sea urchin-like nanospheres have been copiously synthesized [8, 28, 32–37].

Numerous ongoing research efforts based on different types of active species, such as heteroatom containing surface functional groups [38, 39], transition metal oxides [40, 41], and electrically CPs, have been dedicated for the emergence of promising materials to be used in the next-generation energy storage applications [42–44]. Among various metal oxides, such as MnO_2 , V_2O_5 , and RuO_2 etc., Fe_2O_3 has attracted considerable research interest as LIB anode material due to its high theoretical specific capacity (1007 mAh g^{-1}), low-cost and high abundance [41, 45, 46]. However, similar to other metal oxides, Fe_2O_3 also has its own disadvantages, like low electrical conductivity, high cost and poor cycling stability [47], which need to be addressed in order to optimize its electrochemical application performance.

In the current study, a combined method is proposed for the first time synthesis of “carbon or metal oxide nanostructure decorated HCNSs” through a MW energy-based carbonization approach [20], which was simply modified from relevant previous studies [8, 37, 48], as shown in Fig. 1. This approach can be considered more beneficial than the primarily mentioned available methods from many aspects with respect to (i) its high efficiency, selective heating mechanism, simple experimental conditions and instrument setups, (ii) its general route, which is template-free and enables the decoration of various functional nanostructures, i.e., CNTs and MONWs, on the surface of the as-obtained HCNSs, (iii) its way of using CPs as a functional carbon scaffold to provide high environmental stability and electrochemical activity for the composite structure, (iv) its versatility that allows working with different precursors, (v) its possibility to control the uniformity of the nanostructures' radial growth, and mostly importantly, (vi) its ultrafast nature to obtain 3D nanomaterials in a composite form.

Figure 1 Schematic illustration of the CNT-MONW/HCNS composites' preparation.



Experimental

Materials

Following chemicals and reagents, including styrene (99%), ammonium peroxydisulfate (APS, $(\text{NH}_4)_2\text{S}_2\text{O}_8$, 98% min.), ferrocene (99%) and pyrrole (98 + %), were all purchased from Alfa Aesar and used for the synthesis reactions. Sodium dodecyl sulfate (SDS, $\text{C}_{12}\text{H}_{25}\text{NaO}_4\text{S}$, 99%) was purchased from IBI Scientific. Iron pentacarbonyl ($\text{Fe}(\text{CO})_5$, 99.5% and 99%-Fe) was purchased from Strem Chemicals. Ethanol (EtOH, absolute 200 proof) was purchased from Electron Microscopy Sciences (EMS). Tetrahydrofuran (THF) was purchased from BDH. All reagents

were used as-received without further treatment unless otherwise specified.

One-step synthesis of polystyrene latex NSs (PS NSs)

The PS NSs were prepared based on a previously reported method by initially adding 4 mL of styrene monomer into a 250-mL round-bottom flask containing a magnetic stir bar and 80 mL of 3 mM aq. SDS [49]. A reflux condenser was attached to the reaction medium, and the flask was placed in a preheated oil bath at 70 °C for 20 min under high magnetic stir. In the end, 68 mg of the oxidant APS was dissolved in 1 mL H_2O and slowly added into the

monomer dispersion. The polymerization reaction was allowed to proceed for 4 h at 70 °C until yielding a milky suspension. The resulting PS NSs' latex was removed from the heat and allowed to naturally cool down to room temperature before being transferred into a container for storage purposes.

One-step synthesis of PPy-coated PS NSs (PPy/PS NSs)

The as-obtained PS NSs from the previous step were used as substrates, without further purification, to coat conducting PPy on their surfaces via an in situ oxidative polymerization reaction at ambient conditions. Here, in a 100-mL beaker containing 60 mL 1 M aq. HCl, 10 g of PS latex was mixed with 1 mL pyrrole monomer. The solution was stirred for 10 min to allow homogenous distribution of monomers in the solution. The reaction medium was then moved into an ice bath where it was approximately cooled down to 5 °C. The oxidant solution was prepared by firstly dissolving 1.15 g of APS in 10 mL 1 M aq. HCl, then cooling the solution down to 5 °C, and then adding it dropwise into the monomer solution over 10 min under high magnetic stirring. Once the oxidant had been completely added, the reaction was left to proceed for 1 h. The resulting black suspension was first filtered and washed with excess 1 M aq. HCl to remove any unreacted monomer and/or oxidant, and eventually, it was dried overnight under vacuum at 60 °C to yield a fine black PPy/PS powder.

Preparation of hollow PPy NSs (PPy HNSs)

The PS latex cores of PPy/PS NSs were removed by using THF via subsequent carbonization/extraction steps. Here, 5 g of PPy/PS sample was placed in a 20 mL scintillation vial with a loosely attached cap, and then exposed to 1250 W MW power for 10 s to minimally carbonize the PPy coating. This step helps maintaining the samples' spherical shape, while their PS cores are removed. The carbonized NSs were then mixed with 50 mL THF for 30 min at high magnetic stir to remove their PS cores. The etched NSs were collected by filtration and washed with excess THF to remove any PS traces, and finally dried under vacuum at 60 °C.

Preparation of CNT or MONW decorated hollow carbon NSs (CNT-MONW/HCNSs) via rapid microwave (MW) irradiation

To obtain the CNT decorated samples, 50 mg of partially carbonized PPy HNS powder was mixed with ferrocene, which was pre-dissolved in 5 mL EtOH, at 1:1 ratio by using a speed mixer at 3500 rpm. Here, the purpose was to facilitate the penetration of dissolved ferrocene into PPy HNSs. After the evaporation of EtOH from this mixture, ferrocene formed an orange color layer on the surface of dark PPy powder. This solid-state mixture was transferred into a capped glass vial, which was placed into a standard kitchen MW oven (Panasonic Inverter, NN-SN936B) chamber. At 1250 W MW power for 30 s, the sample was irradiated. Upon rapid heat gain through the PPy HNSs: (i) complete carbonization of PPy HNSs was occurred, while (ii) ferrocene got rapidly decomposed and simultaneously formed a gaseous phase, which lead (iii) to the formation/decoration of CNTs, along with continuous sparking on the sample surface. Eventually, the vial was taken out from the MW to cool down to room temperature. The as-obtained sample was collected and stored for further characterization steps.

Similarly, to the above-mentioned system, in order to obtain the MONW decorated samples; the same amount of partially carbonized PPy HNS powder was placed in a glass vial and soaked with $\text{Fe}(\text{CO})_5$ until its surface was completely covered with the chemical (0.1 mL). After the partial evaporation of the liquid phase, the sample was placed in the MW oven chamber for the quick heating process. During 30 s of process time, there were vigorous sparking and glowing observed on the sample surface. Finally, after the vial was taken out and cooled down to room temperature, HCNSs with homogenous iron oxide NW decoration on their surface were gently collected from the vial bottom with a steel spatula and stored for further characterizations.

Characterization of the as-obtained nanocomposites

Different characterization techniques were used in order to identify the as-obtained CNT-MONW/HCNS nanocomposites' properties. Both their morphological and compositional features were analyzed by JEOL JSM-7000F scanning electron microscope

(SEM) equipped with an energy-dispersive X-ray (EDX) detector. The specific surface areas (SSA) of the nanocomposites were calculated by using Brunauer–Emmett–Teller (BET) analysis. Moreover, their in-depth morphological analysis was performed on a JEOL 2100F transmission electron microscope (TEM) that was operated at 200 kV. The major functional groups exist in these nanocomposites were detected by using a Thermo Nicolet 6700 Fourier Transform Infra-Red (FT-IR) spectroscope. The as-obtained nanocomposites' thermal stability was characterized by using thermal gravimetric analysis (TGA) performed on a TA Q2000 system from room temperature up to 800 °C (at 10 °C min⁻¹ heating rate, in O₂ atmosphere). Additionally, the crystalline nature of the as-formed MONWs on HCNSs was determined by X-ray diffractometry (XRD) analysis, which was performed on a Rigaku powder XRD instrument.

Results and discussion

For the above-mentioned synthesis reactions, the as-used SDS amount was varied to reveal its effect on the as-obtained NSs' size dependency (Fig. 2, Table 1). After these PS latex NS samples were coated with PPy, their diameter values were increased ~ 20 nm (80–240 nm).

Figure 2 SEM images of the as-synthesized PS NSs with varied concentrations; **a** 1.5 mM, **b** 2 mM, **c** 3 mM, and **d** 6.5 mM of SDS, respectively.

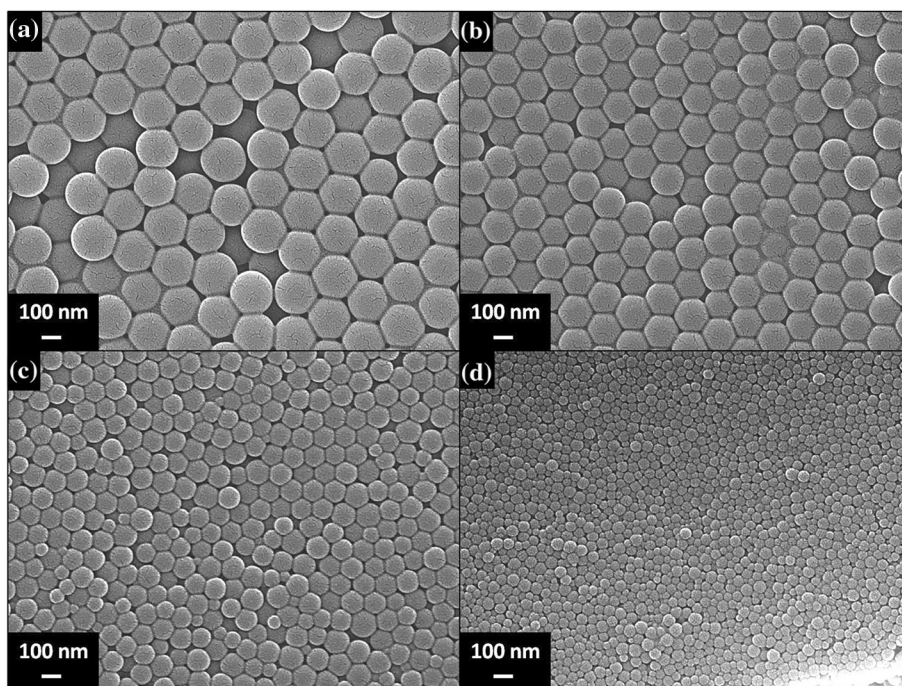


Table 1 Summary of the as-obtained PS NSs' average diameter values with varying SDS concentration

SDS concentration (mM)	PS NS diameter (nm)
6.5	~ 60
3	110
2	180
1.5	220

Here, the largest PS NSs were used as templates to prepare the PPy HNSs (Fig. 3a). As can be seen from Fig. 3, the PPy HNSs were prepared by first, applying short-term MW energy for both partial surface carbonization and to retain the spherical morphology during the subsequent extraction step, and then applying THF extraction to these partially carbonized samples (Fig. 3b, c). Since their PS cores were removed under high magnetic stirring, such HNSs seem like vacuumed from one side (Fig. 3d). The resulting PPy HNSs appeared as fine black powders after the removal of their PS cores and drying.

The present major functional groups' verification and the thermal stability analysis of the as-synthesized NSs were conducted by using FT-IR and TGA characterizations, respectively. The FT-IR results shown in Fig. 4 and summarized in Table 2 indicate that PPy/PS NS sample was successfully synthesized

Figure 3 SEM images of the; **a** PS NSs, **b** PPy/PS NSs, **c** partially carbonized PPy/PS NSs, and **d** PPy HNSs after THF extraction.

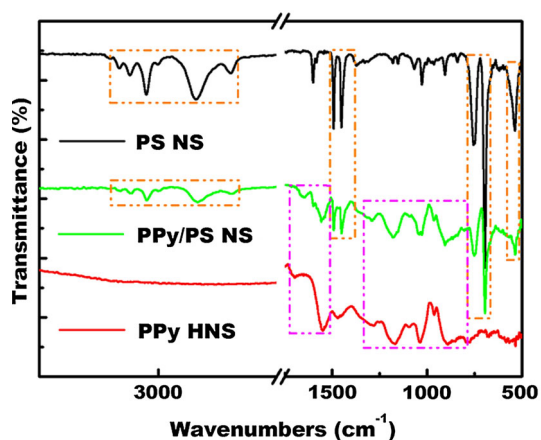
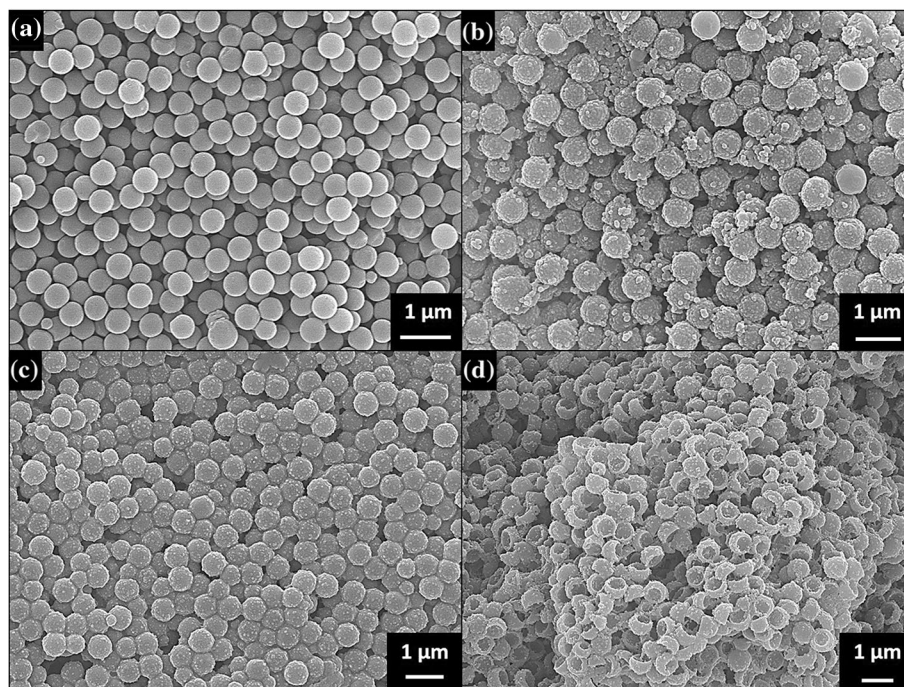


Figure 4 FT-IR spectra of the as-synthesized PS NS, PPy/PS NS and PPy HNS samples.

in a hybrid nanocomposite form and exhibited both of its components' characteristic peaks, which were already presented in relevant previous literature [24, 31].

The PPy/PS NS sample's thermal features also exhibited both of its components' characteristics as can be seen on its TGA thermogram shown in Fig. 5. As indicated by the first purple circle, up to 225 °C, this sample went through ~ 2.5% weight loss, which was caused by the removal of moisture content, the dopants and the low molecular weight heteroatoms, respectively, from its PPy component. The next two

orange circles between 325 and 425 °C indicate the second major weight loss (78%) occurred in PPy/PS NS sample, which was caused by the thermal decomposition of this sample's PS component. The last ~ 14.4% weight loss, occurred between 425 and 600 °C, indicates the completion of PPy content's thermal decomposition (purple circle) in this sample.

Next, the as-prepared CNT-MONW/HCNS samples' morphological features were characterized by using electron microscopy techniques and the results are presented in Figs. 6 and 7, respectively. SEM image of the CNT/HCNSs sample that was prepared through short-term MW energy-based Poptube approach is shown in Fig. 6a. Based on the initial analysis of this image, it can be observed that micron long, bamboo shoot or earth worm-like [36, 50] CNTs were successfully grown at carbonized HNSs' cluster surface. In addition, the as-grown CNTs' coverage density is seemed to be very homogenous, which is a crucial factor for the future application performance of this sample. In Fig. 6b, c, the as-prepared MONW/HCNS composites' overall morphology is exhibited. Compared to the CNT/HCNS sample, the spaghetti-like MONWs grown at the HCNS cluster surface are much longer and their surface coverage is much denser, as well. In Fig. 6d, detailed view of the MONW decorated HCNSs exist in the cluster can be clearly observed. Such nanocomposite structures can

Table 2 Summary of the common FT-IR spectra peaks detected in PS/PPy NS sample shown in Fig. 4

Peak's origin	Wavenumber (cm ⁻¹)	Definition
From PS	3080, 3055, 3025	Aromatic =C–H stretching vibrations
	2920, 2850	Alkyl C–H stretching vibrations
	1490, 1450	Aromatic –C=C– stretching vibrations
	755	Aromatic =C–H out-of-plane deformation vibrations
	700, 535	Out-of-plane ring deformation vibrations
From PPy	1555	Secondary amine N–H peak of pyrrole ring
	1470	Aromatic C–N stretching of pyrrole ring
	1290	C–N ⁺ –H stretching vibrations in pyrrole ring
	1190	C–H in-plane vibrations
	1075	N–H in-plane vibrations (doped state PPy presence)
	905	C–H out-of-plane vibrations

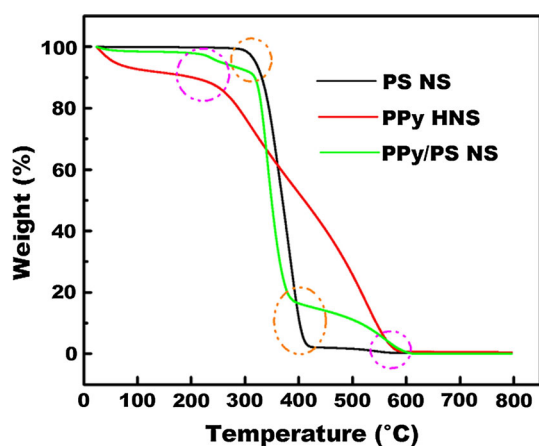
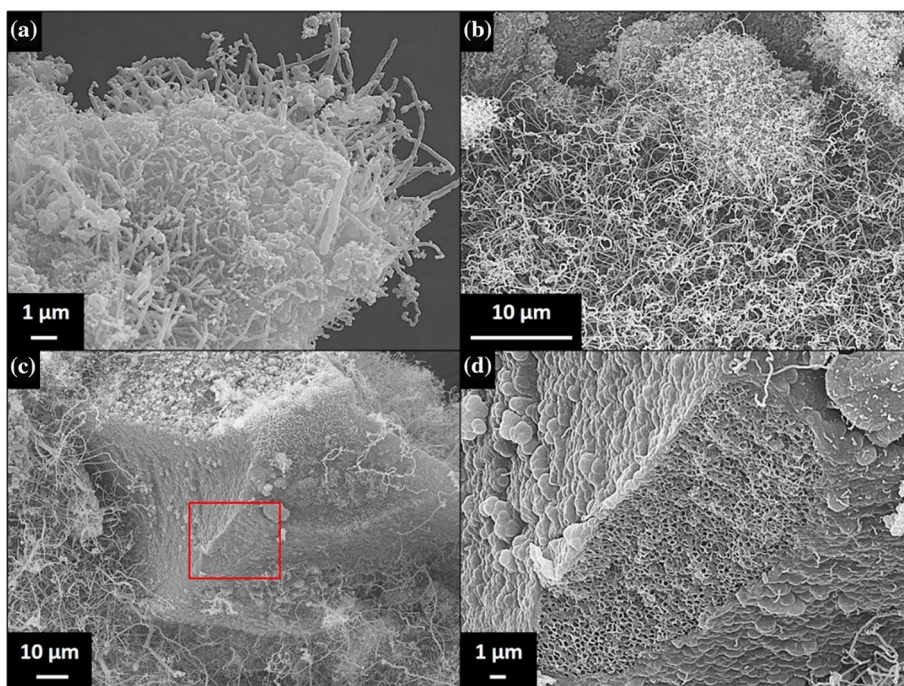


Figure 5 TGA thermograms of the as-synthesized PS NS, PPy/PS NS and PPy HNS samples.

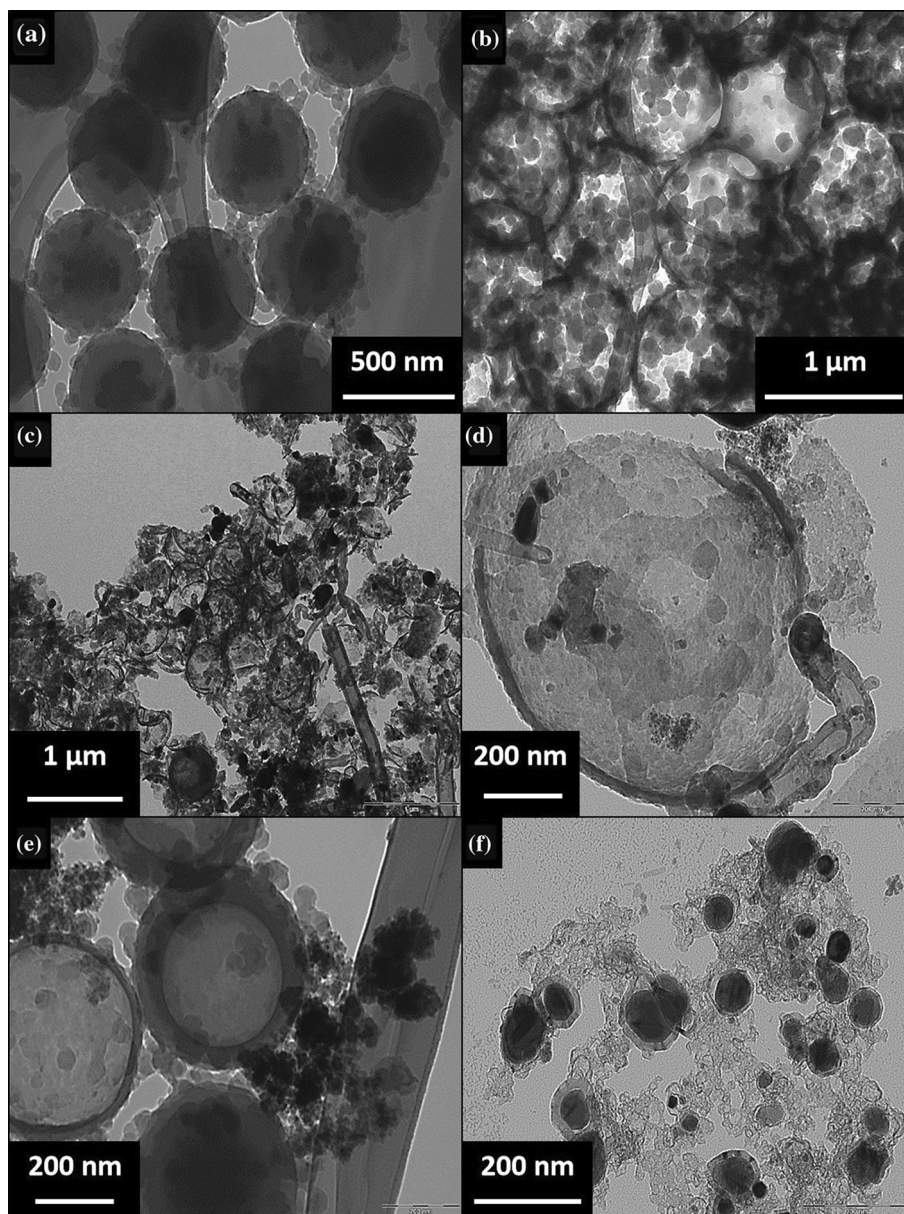
Figure 6 SEM images of; **a** CNT/HCNSs, **b**, **c** MONW/HCNSs, and **d** the marked area's detailed view in (c).



be effectively used for both water treatment and energy storage applications with respect to their ultra-high specific active surface area that is supported by the as-grown microns long iron oxide NWs [8].

The in-depth morphological analyses of the as-prepared samples were done by using TEM imaging technique. Expectedly, the results presented in Fig. 7 are in good agreement with the ones obtained from SEM characterization. PPy/PS NSs can be seen in Fig. 7a. These NSs have a pretty uniform size distribution that ranges between 600 and 650 nm. PPy nanogranule clusters, which were composed of nanogranules with ~ 50 nm average diameter, covering these NSs' surface can be also observed from

Figure 7 TEM images of; **a** PPy/PS NSs, **b** PPy HNSs, **c** CNT/HCNS, **d** a tip-grown, single CNT with bamboo shoot-like hollow stem and an encapsulated Fe NP at its tip, attached to a HCNS, **e** MONW/HCNS, and **f** the core-shell constituents of the as-grown MONWs.

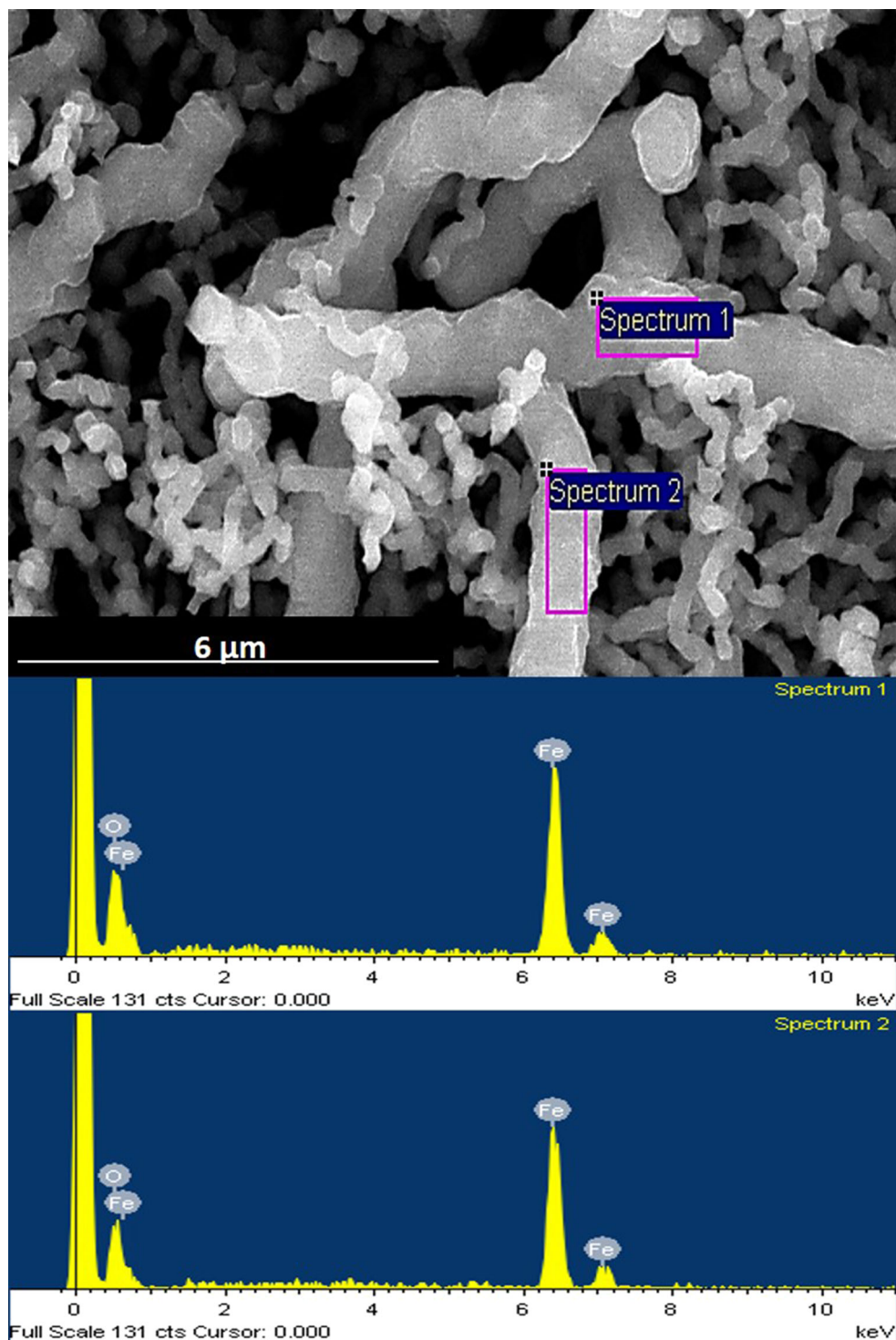


this image. PPy HNSs with ~ 600 nm average diameter can be observed in Fig. 7b. The dense PPy coverage at these HNSs' surface is also obvious in this image. CNT decorated and carbonized versions of the same HNSs can be seen in Fig. 7c, in which such HCNSs and their CNT decoration are seem to be broken probably because of the ultrasonication-based sample preparation step applied prior to TEM imaging. Similarly, in Fig. 7d, a HCNS seems attached to a tip-grown CNT with a bamboo shoot-like hollow stem. Based on the measurements taken on this image, it can be observed that; (i) the HCNS is ~ 600 nm in diameter, (ii) the CNT has ~ 750 nm

long hollow stem and ~ 80 nm in diameter, and (iv) CNT's encapsulated iron nanoparticle (NP) tip is ~ 100 nm in diameter. These results are also strongly supported by the ones obtained from the relevant previous studies, as well [28, 36, 50–52].

Differently from their CNT/HCNS equivalents, MONW/HCNS composite samples were observed to have tiny core-shell NP decoration on their surface rather than MONWs, as can be seen in Fig. 7e. Such NPs were made up of Fe_2O_3 cores that were encapsulated within graphitized carbon shells (Fig. 7f). The reason of this look is believed to be simply related with the disintegration of microns long, web-like

Figure 8 EDX analysis results of the MONWs obtained from $\text{Fe}(\text{CO})_5$ system.

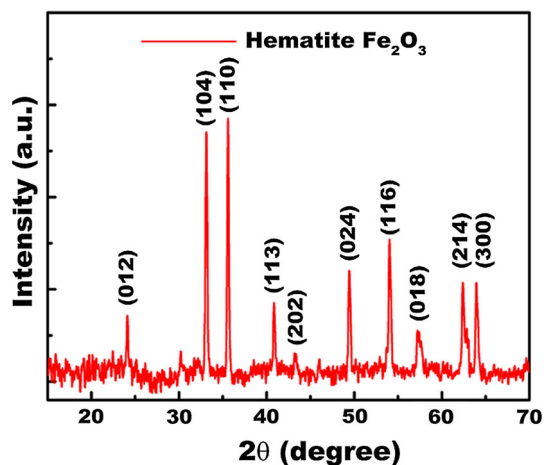


MONWs into its constituents, most probably by the above-mentioned ultrasonication-based sample preparation process. This result agrees well with the ones from the relevant previous studies, in which the NWs obtained from $\text{Fe}(\text{CO})_5$ do not have solid and continuous structures. Instead, these NWs exhibit a

pearl necklace-like morphology that is composed of adjacent NPs encapsulated within graphitized carbon layers [8, 28, 37, 53, 54]. Based on the measurements taken, it was observed that such NPs' diameter size distribution ranges between 40 and 160 nm.

Table 3 Summary of the EDX analysis results shown in Fig. 8

Spectrum	Fe (wt%)	O (wt%)	Total
1	67.47	32.53	100
2	58.32	41.68	100

**Figure 9** X-ray diffractogram of the as-grown MONWs in MONW/HCNS sample.

The as-obtained nanostructures' BET analysis results revealed that HCNSs have the SSA of $80 \text{ m}^2/\text{g}$, whereas the CNT-MONW/HCNS samples have the SSA of $\sim 40 \text{ m}^2/\text{g}$. The as-grown CNTs and MONWs on the HCNSs' surface were expected to increase the overall SSA values, but interestingly, they turn out to have a negative contribution on them. There are two plausible explanations for this phenomenon. The first one is related with the conversion rate of ferrocene into CNTs, which seem to be lower than 100%. In this case, the remaining unconverted ferrocene that stayed on the HCNSs' surface in either amorphous carbon or oxidized iron forms, have only increased the sample's total weight instead of its SSA. The second one is related with the abundance of Fe in both samples, either as incorporated on CNTs or as grown in oxidized NWs form. Similarly, to the former case, such Fe presence has only increased the samples' weight but not their surface area, and thus, causing a significant reduction in their overall SSA values.

Last but not the least, besides the morphological property characterization of the as-prepared MONW/HCNS composite, its elemental composition was also investigated by using EDX analysis.

According to the results, which are summarized from the spectra in Fig. 8, shown in Table 3, it is obvious that the as-grown MONWs at HCNSs' surface are made up of Fe and O elements.

Additionally, in order to identify these MONWs' crystalline nature, XRD analysis was performed on the relevant sample. It can be observed in Fig. 9 that characteristic diffraction peaks appeared on the as-grown MONWs' spectrum was matching with the standard Fe_2O_3 hematite (JCPDS: 33-0664) [8, 28].

Conclusion

The following aspects can be listed as the particular interest of this study: (i) conducting well-established and cutting-edge experimental studies, preferably with the previous literature verification, (ii) development of new multifunctional materials with a vast potential for advanced engineering applications, (iii) characterization of the structure and chemistry of the as-obtained materials to understand their various features, and (iv) elucidation of the efficient mechanisms involved in the synthesis and processing of the as-obtained nanocomposites as a route to determine their applications.

Thus, according to these interests, the synthesis of CNT or MONW decorated HCNSs was achieved throughout this study. Two well-established methods, namely polymeric latex NS synthesis and MW energy-based Poptube, were combined for the success of this approach, which is strongly supported by both various material characterization test results and the previous literature data. Besides, the as-synthesized HCNSs through this approach are more advantageous than the previously presented ones in the literature, with respect to: (i) their simple, facile, easily scalable and low-cost combined synthesis method and (ii) their enhanced application potential due to the as-grown CNT and MONW decorations on their surface, which provide both ultra-high specific active surface area and relevant properties of these components to the nanostructure. In conclusion, it is believed that the as-obtained CNT-MONW/HCNS nanocomposites will soon become the materials of preference for various advanced applications such as energy harvesting/storage, magnetic resonance imaging (MRI), water treatment and drug delivery.

Acknowledgements

The authors gratefully acknowledge the financial support from USDA-NIFA and Namik Kemal University scientific research award NKUBAP.00.17.AR.15.04.

References

- [1] Lou XW, Archer LA, Yang ZC (2008) Hollow micro-/nanostructures: synthesis and applications. *Adv Mater* 20:3987–4019
- [2] Kim M, Sohn K, Bin Na H, Hyeon T (2002) Synthesis of nanorattles composed of gold nanoparticles encapsulated in mesoporous carbon and polymer shells. *Nano Lett* 2:1383–1387
- [3] Kamata K, Lu Y, Xia YN (2003) Synthesis and characterization of monodispersed core-shell spherical colloids with movable cores. *J Am Chem Soc* 125:2384–2385
- [4] Liu N, Wu H, McDowell MT, Yao Y, Wang CM, Cui Y (2012) A yolk-shell design for stabilized and scalable Li-ion battery alloy anodes. *Nano Lett* 12:3315–3321
- [5] Zheng GY, Zhang QF, Cha JJ, Yang Y, Li WY, Seh ZW et al (2013) Amphiphilic surface modification of hollow carbon nanofibers for improved cycle life of lithium sulfur batteries. *Nano Lett* 13:1265–1270
- [6] Ikeda S, Ishino S, Harada T, Okamoto N, Sakata T, Mori H et al (2006) Ligand-free platinum nanoparticles encapsulated in a hollow porous carbon shell as a highly active heterogeneous hydrogenation catalyst. *Angew Chem Int Ed* 45:7063–7066
- [7] Zhang WM, Hu JS, Guo YG, Zheng SF, Zhong LS, Song WG et al (2008) Tin-nanoparticles encapsulated in elastic hollow carbon spheres for high-performance anode material in lithium-ion batteries. *Adv Mater* 20:1160–1165
- [8] Liu Z, Chen L, Zhang L, Poyraz S, Guo ZH, Zhang XY et al (2014) Ultrafast Cr(VI) removal from polluted water by microwave synthesized iron oxide submicron wires. *Chem Commun* 50:8036–8039
- [9] Fuertes AB, Sevilla M, Valdes-Solis T, Tartaj P (2007) Synthetic route to nanocomposites made up of inorganic nanoparticles confined within a hollow mesoporous carbon shell. *Chem Mater* 19:5418–5423
- [10] Jayaprakash N, Shen J, Moganty SS, Corona A, Archer LA (2011) Porous hollow carbon@sulfur composites for high-power lithium-sulfur batteries. *Angew Chem Int Ed* 50:5904–5908
- [11] Yang SB, Feng XL, Zhi LJ, Cao QA, Maier J, Mullen K (2010) Nanographene-constructed hollow carbon spheres and their favorable electroactivity with respect to lithium storage. *Adv Mater* 22:838–842
- [12] Zhang CF, Wu HB, Yuan CZ, Guo ZP, Lou XW (2012) Confining sulfur in double-shelled hollow carbon spheres for lithium-sulfur batteries. *Angew Chem Int Ed* 51:9592–9595
- [13] Caruso F, Spasova M, Susha A, Giersig M, Caruso RA (2001) Magnetic nanocomposite particles and hollow spheres constructed by a sequential layering approach. *Chem Mater* 13:109–116
- [14] Jang J, Ha H (2003) Fabrication of carbon nanocapsules using PNMA/PDVB core/shell nanoparticles. *Chem Mater* 15:2109–2111
- [15] Lu AH, Li WC, Hao GP, Spliethoff B, Bongard HJ, Schaack BB et al (2010) Easy synthesis of hollow polymer, carbon, and graphitized microspheres. *Angew Chem Int Ed* 49:1615–1618
- [16] Wang ZF, Mao PF, He NY (2006) Synthesis and characteristics of carbon encapsulated magnetic nanoparticles produced by a hydrothermal reaction. *Carbon* 44:3277–3284
- [17] Qiao SZ, Lin CX, Jin YG, Li Z, Yan ZM, Hao ZP et al (2009) Surface-functionalized periodic mesoporous organosilica hollow spheres. *J Phys Chem C* 113:8673–8682
- [18] Xu LQ, Zhang WQ, Yang Q, Ding YW, Yu WC, Qian YT (2005) A novel route to hollow and solid carbon spheres. *Carbon* 43:1090–1092
- [19] Katcho NA, Urones-Garrote E, Avila-Brandé D, Gomez-Herrero A, Urbonaité S, Csillag S et al (2007) Carbon hollow nanospheres from chlorination of ferrocene. *Chem Mater* 19:2304–2309
- [20] Zhang XY, Manohar SK (2006) Microwave synthesis of nanocarbons from conducting polymers. *Chem Commun* 23:2477–2479
- [21] Fujii S, Matsuzawa S, Nakamura Y (2010) One-pot synthesis of conducting polymer-coated latex particles: ammonium persulfate as free radical initiator and chemical oxidant. *Chem Commun* 46:7217–7219
- [22] Poyraz S, Flogel M, Liu Z, Zhang XY (2017) Microwave energy assisted carbonization of nanostructured conducting polymers for their potential use in energy storage applications. *Pure Appl Chem* 89:173–182
- [23] Zhang L, Du W, Nautiyal A, Liu Z, Zhang XY (2018) Recent progress on nanostructured conducting polymers and composites: synthesis, application and future aspects. *Sci China Mater* 61:303–352
- [24] Zhang JR, Qiu T, Ren SS, Yuan HF, He LF, Li XY (2012) Simple synthesis of polypyrrole-polystyrene hybrid hollow spheres. *Mater Chem Phys* 134:1072–1078
- [25] Chang CH, Son PS, Yoon JA, Choi SH (2010) Synthesis of hollow conductive polypyrrole balls by the functionalized polystyrene as template. *J Nanomater* 168025:1–6

- [26] Fu JW, Xu Q, Chen JF, Chen ZM, Huang XB, Tang XZ (2010) Controlled fabrication of uniform hollow core porous shell carbon spheres by the pyrolysis of core/shell polystyrene/cross-linked polyphosphazene composites. *Chem Commun* 46:6563–6565
- [27] Fang B, Kim JH, Kim MS, Bonakdarpour A, Lam A, Wilkinson DP et al (2012) Fabrication of hollow core carbon spheres with hierarchical nanoarchitecture for ultrahigh electrical charge storage. *J Mater Chem* 22:19031–19038
- [28] Liu Z, Zhang L, Poyraz S, Smith J, Kushvaha V, Tippur H et al (2014) An ultrafast microwave approach towards multicomponent and multi-dimensional nanomaterials. *RSC Adv* 4:9308–9313
- [29] Fujii S, Matsuzawa S, Nakamura Y, Ohtaka A, Teratani T, Akamatsu K et al (2010) Synthesis and characterization of polypyrrole-palladium nanocomposite-coated latex particles and their use as a catalyst for Suzuki coupling reaction in aqueous media. *Langmuir* 26:6230–6239
- [30] Malinauskas A (2001) Chemical deposition of conducting polymers. *Polymer* 42:3957–3972
- [31] Cho SH, Kim WY, Jeong GK, Lee YS (2005) Synthesis of nano-sized polypyrrole-coated polystyrene latexes. *Colloids Surf A Physicochem Eng Asp* 255:79–83
- [32] Liu Z, Liu Y, Poyraz S, Zhang XY (2011) Green-nano approach to nanostructured polypyrrole. *Chem Commun* 47:4421–4423
- [33] Zhang XY, Manohar SK (2004) Bulk synthesis of polypyrrole nanofibers by a seeding approach. *J Am Chem Soc* 126:12714–12715
- [34] Zhang XY, Manohar SK (2005) Narrow pore-diameter polypyrrole nanotubes. *J Am Chem Soc* 127:14156–14157
- [35] Liu Z, Zhang XY, Poyraz S, Surwade SP, Manohar SK (2010) Oxidative template for conducting polymer nanocaps. *J Am Chem Soc* 132:13158–13159
- [36] Liu Z, Wang JL, Kushvaha V, Poyraz S, Tippur H, Park S et al (2011) Poptube approach for ultrafast carbon nanotube growth. *Chem Commun* 47:9912–9914
- [37] Zhang XY, Liu Z (2012) Recent advances in microwave initiated synthesis of nanocarbon materials. *Nanoscale* 4:707–714
- [38] Hulicova D, Kodama M, Hatori H (2006) Electrochemical performance of nitrogen-enriched carbons in aqueous and non-aqueous supercapacitors. *Chem Mater* 18:2318–2326
- [39] Liu Z, Zhang L, Poyraz S, Zhang XY (2013) Conducting polymer—metal nanocomposites synthesis and their sensory applications. *Curr Org Chem* 17:2256–2267
- [40] Hu CC, Chang KH, Lin MC, Wu YT (2006) Design and tailoring of the nanotubular arrayed architecture of hydrous RuO₂ for next generation supercapacitors. *Nano Lett* 6:2690–2695
- [41] Zhang LL, Li S, Zhang JT, Guo PZ, Zheng JT, Zhao XS (2010) Enhancement of electrochemical performance of macroporous carbon by surface coating of polyaniline. *Chem Mater* 22:1195–1202
- [42] Kelly TL, Yano K, Wolf MO (2009) Supercapacitive properties of PEDOT and carbon colloidal microspheres. *ACS Appl Mater Interfaces* 1:2536–2543
- [43] Lei ZB, Chen ZW, Zhao XS (2010) Growth of polyaniline on hollow carbon spheres for enhancing electrocapacitance. *J Phys Chem C* 114:19867–19874
- [44] Chen Z, Qin YC, Weng D, Xiao QF, Peng YT, Wang XL et al (2009) Design and synthesis of hierarchical nanowire composites for electrochemical energy storage. *Adv Func Mater* 19:3420–3426
- [45] Yang SB, Feng XL, Ivanovici S, Mullen K (2010) Fabrication of graphene-encapsulated oxide nanoparticles: towards high-performance anode materials for lithium storage. *Angew Chem Int Ed* 49:8408–8411
- [46] Lai XY, Halpert JE, Wang D (2012) Recent advances in micro-/nano-structured hollow spheres for energy applications: from simple to complex systems. *Energy Environ Sci* 5:5604–5618
- [47] Kang LT, Xie LL, Li PY, Liu TJ, Zhang XY, Luo JJ et al (2015) One-step combustion synthesis of CNTs doped Fe₂O₃/C nanocomposites as electrode materials for supercapacitors. *Fuller Nanotubes Carbon Nanostruct* 23:715–720
- [48] Raymundo-Pinero E, Cadek M, Beguin F (2009) Tuning carbon materials for supercapacitors by direct pyrolysis of seaweeds. *Adv Func Mater* 19:1032–1039
- [49] Zhenxing H, Xiaowei Y, Junliang L, Yuping Y, Ling W, Yanwei Z (2011) An Investigation of the effect of sodium dodecyl sulfate on quasi-emulsifier-free emulsion polymerization for highly monodisperse polystyrene nanospheres. *Eur Polymer J* 47:24–30
- [50] Poyraz S, Zhang L, Schroder A, Zhang XY (2015) Ultrafast microwave welding/reinforcing approach at the interface of thermoplastic materials. *ACS Appl Mater Interfaces* 7:22469–22477
- [51] Poyraz S, Liu Z, Liu Y, Zhang XY (2013) Devulcanization of scrap ground tire rubber and successive carbon nanotube growth by microwave irradiation. *Curr Org Chem* 17:2243–2248
- [52] Xie H, Poyraz S, Thu M, Liu Y, Snyder EY, Smith JW et al (2014) Microwave-assisted fabrication of carbon nanotubes decorated polymeric nano-medical platforms for simultaneous drug delivery and magnetic resonance imaging. *RSC Adv* 4:5649–5652
- [53] Liu Z, Zhang L, Wang RG, Poyraz S, Cook J, Bozack MJ et al (2016) Ultrafast microwave nano-manufacturing of fullerene-like metal chalcogenides. *Sci Rep* 6:22503–22510
- [54] Schwenke AM, Hoepfener S, Schubert US (2015) Synthesis and modification of carbon nanomaterials utilizing microwave heating. *Adv Mater* 27:4113–4141